



Sol-gel synthesis and characterization of $\text{Co}_3\text{O}_4/\text{CeO}_2$ nanocomposites and its application for photocatalytic discoloration of organic dye from aqueous solutions

Mohammad Hassanpour¹ · Masoud Salavati-Niasari¹ · Hossein Safardoust-Hojaghan¹

Received: 14 May 2020 / Accepted: 28 September 2020 / Published online: 6 October 2020
© Springer-Verlag GmbH Germany, part of Springer Nature 2020

Abstract

Herein, $\text{Co}_3\text{O}_4/\text{CeO}_2$ nanocomposite was synthesized by the modified Pechini method. Citric, maleic, succinic, and trimesic acids were used as a stabilizer, and the variation affected the morphology and size of the synthesized nanocomposites. Subsequently, the formation of $\text{Co}_3\text{O}_4/\text{CeO}_2$ nanocomposites was confirmed by various analyses. Furthermore, the particles were considered for size and morphology by SEM and HRTEM analyses, and the sample that used trimesic acid as the stabilizer was designated as the goal sample to continue the route. The optimum sample was used to investigate the photocatalytic properties of the synthesized nanocomposite. The UV-light photocatalyst test was performed in neutral, alkaline, and acidic states against two aqueous solutions containing color contamination of methylene blue and erythrosine B dyes. The results showed decolorization at 85% for methylene blue and 90% for erythrosine B over 120 min test time.

Keywords Sol-gel · $\text{Co}_3\text{O}_4/\text{CeO}_2$ · Nanocomposite · Photocatalyst · Water pollutants

Introduction

Environmental pollution by various factors has involved much notice in recent decades and the pollution of aquatic environments due to the importance of water to humans has caused great concern in different societies (Khan and Malik 2019; Wutich 2019). Due to the importance of sanitizing water from the substances that cause it unhealthy, many researchers have attracted the attention of researchers to remove these contaminants in rapid and inexpensive methods (Fernández et al. 2016; Kumar Reddy and Lee 2012; Pradeep 2009; Qin et al. 2019). Nano-sized materials, as a new group of materials that have been used extensively in the past decades due to their unique properties, are among the materials that are of interest to researchers working on water treatment (Ghasali et al. 2020; Karimi-Maleh et al. 2020a; Karimi-Maleh et al. 2020b; Orooji et al. 2019a, 2019b, 2019c; Santhosh et al. 2019; Sisi et al. 2020; Wang 2019; Arefi-Oskoui

et al. 2019). The photocatalytic process on semiconductors materials is one of the paths that researchers take to remove organic compounds and some other water contaminants by nanomaterials (Belver et al. 2019; Ghasemi et al. 2020; Rad et al. 2020; Zhang et al. 2019). Metal oxide nanocomposites have semiconductor properties. These materials are among the most commonly used materials for the photocatalytic process (Alem et al. 2020; Boruah et al. 2019; Kumar and Rao 2017).

Recently, mix metal oxides due to their mix properties have received a lot of attention and researches have shown that when two or more metal oxides are put together, the features that appear are either complementary to the effects of each metal oxide or, in some cases, reduce some of the individual properties of metal oxide, which is useful in any way to attain the desired goals (Fuku et al. 2018; Hassanpour et al. 2017b; Karthik et al. 2018; Mousavi et al. 2018; Orooji et al. 2020; Qi et al. 2015; Reddy et al. 2018; Zhao et al. 2018; Zhu et al. 2012). For instance, Guo et al. (2015) who prepared multi-layer hollow CuO@NiO spheres for storage goal, which is due to its structural characteristics, showed a large higher-than-theoretical capacity that is very excellent among various NiO or CuO electrode structures. Singh et al. (2013) synthesized porous ZnO embedded with Fe_3O_4 nanoparticles to form $\text{Fe}_3\text{O}_4\text{-ZnO}$ magnetic semiconductor nanocomposites; they recorded that prepared nanocomposites have much better

Responsible Editor: Sami Rtimi

✉ Masoud Salavati-Niasari
salavati@kashanu.ac.ir

¹ Institute of Nano Science and Nano Technology, University of Kashan, P.O. Box 87317-51167, Kashan, Islamic Rep, Iran

attractive features for the purification of wastewater as compared with individual oxides. Wei et al. (2019) synthesized the broccoli-like $\text{SrTiO}_3\text{-TiO}_2$ heterogeneous hollow multi-shelled structures. They reported that, in addition to the special role of morphology in light absorption property of catalysts, the structure of the $\text{SrTiO}_3\text{-TiO}_2$ junctions enhanced the separation performance of the photogenerated charge carriers.

Among the nano-scale metal oxides, transition metal oxides are one of the most widely used materials, and one of these well-known metal oxides is Co_3O_4 . Many uses have been reported for cobalt oxides, such as catalyst (Dong et al. 2007), supercapacitors (Vijayakumar et al. 2013; Orooji et al. 2019a, 2019b, 2019c), anodes for lithium-ion batteries (Wang et al. 2015), gas sensors (Li et al. 2005), magnetic materials (Makhlouf 2002), and photocatalyst (Hassanpour et al. 2017a; Soofivand and Salavati-Niasari 2015; Warang et al. 2013). On the other hand, CeO_2 is one of the well-known rare-earth oxides that have interesting applications in sensors (Fu et al. 2007), catalysts (Li et al. 2019), anti-bacterial (Kannan and Sundrarajan 2014), and photocatalyst (Hassanpour et al. 2018; Liyanage et al. 2014; Qi et al. 2014; Zhai et al. 2007; Hassandoost et al. 2019). For both of these oxides, there are many reports of their combination with other metal oxides in the literature. For example, Li and Yan (2009) prepared $\text{CeO}_2\text{-Bi}_2\text{O}_3$ with a hydrothermal approach and used the obtained microstructures for photocatalytic degradation of RhB. They concluded that when two metal oxides are combined, the photocatalytic activity increased than when they are used separately. Fiorenza et al. (2018) synthesized macro-mesoporous $\text{TiO}_2\text{-CeO}_2$ and examined its photocatalytic activity, revealing that when the amount of the CeO_2 was low, the photocatalytic activity increased. Wang et al. synthesized the hollow multishelled structure of $\text{Co}_3\text{O}_4\text{-CeO}_{2-x}$ nanocomposites for CO catalytic oxidation. The specific morphology of this nanocomposite greatly influenced the creation of active sites to advance the catalytic process (Wang et al. 2019). Because of the amazing results stated, the synthesis of binary metal oxides attracted our attention.

In this work, for the first one, $\text{Co}_3\text{O}_4/\text{CeO}_2$ nanocomposites were synthesized by an informal modified Pechini method using carboxylic acid as a stabilizer and a diol as a polymerization agent. After testing the effect of the type of carboxylic acid on size and morphology, the optimal sample was used for the decolorization of water pollutants in photocatalyst tests. The impure water included methylene blue (MB) and erythrosine (ET) colors.

Experimental

Materials and method

$\text{Ce}(\text{NO}_3)_3 \cdot 6\text{H}_2\text{O}$, $\text{Co}(\text{NO}_3)_2 \cdot 6\text{H}_2\text{O}$, propylene glycol (PG), and liquor ammonia solution containing 25% NH_3 and

citric, maleic, succinic, and trimesic acids were purchased from Merck, and all the chemicals were used as received without further purifications. The XRD patterns were recorded by a Philips X-ray diffractometer using Ni-filtered $\text{CuK}\alpha$ radiation. Fourier transform infrared (FTIR) spectra were detected by means of Nicolet Magna-550 spectrometer in KBr pellets. The UV–vis diffuse reflectance analysis of the as-prepared $\text{Co}_3\text{O}_4/\text{CeO}_2$ nanocomposites was done by applying a UV–vis spectrophotometer (Shimadzu, UV-2550, Japan). SEM images were obtained using a TESCAN instrument model Mira3 to take images, and the samples were coated by a very thin layer of Pt to make the sample surface conductor and prevent charge accumulation, obtaining a better contrast. Transmission electron microscopy (TEM) image was achieved via a Philips EM208 transmission electron microscope with an accelerating voltage of 200 kV. GC-2550TG (Teif Gostar Faraz Company, Iran) was used for all chemical analyses. The Brunauer–Emmett–Teller method (BET) was used to determine the specific surface areas of the catalysts. The measurements were carried out with a Belsorp mini II device at the boiling temperature of liquid nitrogen (-196°C). Pore size distribution was calculated by using the desorption branch of the isotherm by the Barrett, Joyner, and Halenda (BJH) method. Magnetic properties were measured using a vibrating sample magnetometer 60 (VSM, Meghnatis Kavir Kashaan Co., Kashaan, Iran).

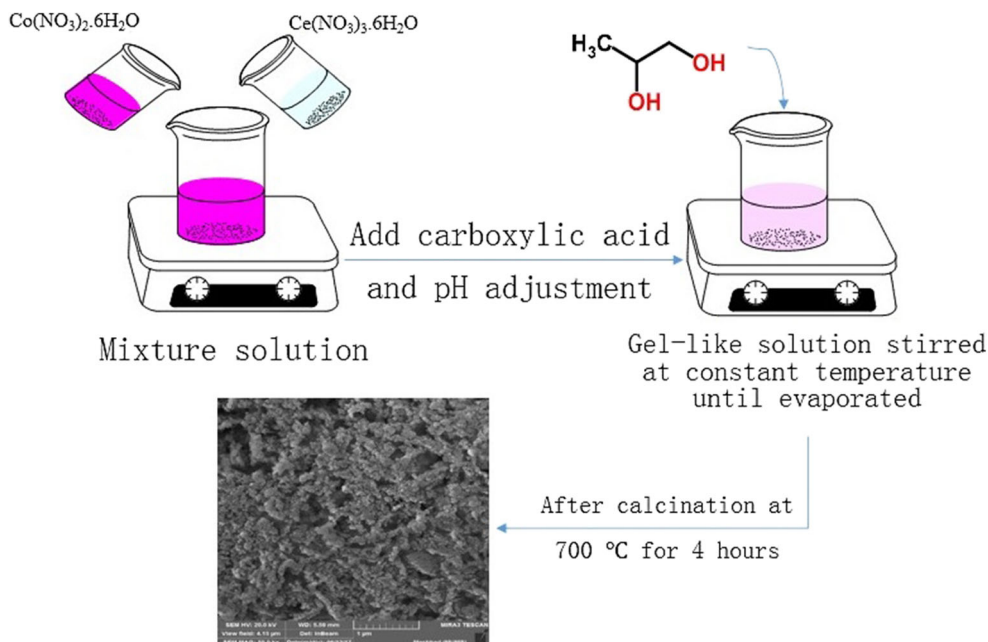
Synthesis of $\text{Co}_3\text{O}_4/\text{CeO}_2$ nanocomposites

For synthesis of $\text{Co}_3\text{O}_4/\text{CeO}_2$ nanocomposites in a modified Pechini method, 0.001 mol of each $\text{Ce}(\text{NO}_3)_3 \cdot 6\text{H}_2\text{O}$ and $\text{Co}(\text{NO}_3)_2 \cdot 6\text{H}_2\text{O}$ was dissolved in distilled water. After that, 0.002 mol of carboxylic acid was added into the previous solution. Also, by adding NH_3 , the pH of the solution was arranged to 6. Then, 0.012 mol of PG as a polymerization agent was added to the mixture solution. The obtained solution at a constant temperature, stirred until the resultant gel-like solution becomes solid sediment, was evaporated. After that, to gain $\text{Co}_3\text{O}_4/\text{CeO}_2$ nanocomposites, the solid sediment was calcined at 700°C for 4 h. The effects of different stabilizing agents, on the size and morphology of the $\text{Co}_3\text{O}_4/\text{CeO}_2$ nanocomposites, were studied. Figure 1 illustrates the schematic of the synthesis route briefly.

Preparation of photocatalytic test

The photocatalytic activity of the $\text{Co}_3\text{O}_4/\text{CeO}_2$ nanocomposites was applied by controlling the decolorization of dye in aqueous solution, under irradiation with UV light. Photocatalytic decolorization was performed with a 5 ppm solution of dyes and 0.05 g of nanocomposites. Then, the

Fig. 1 Schematic of $\text{Co}_3\text{O}_4/\text{CeO}_2$ nanocomposite synthesis route



solution was placed in a photoreactor under UV light and stirred for 20 min at dark to ensure the appropriate adsorption-desorption equilibrium of the dye molecules on the surface of the nanostructures required to perform as an effective photocatalyst. To maintain the solution's saturated oxygen throughout the reaction, the air was blown into the container via a pump. Then, $\text{Co}_3\text{O}_4/\text{CeO}_2$ was separated from the 5 ml samples, taken from the degraded solution at various time intervals, using 5 min centrifuging at 12,000 rpm. The dye concentration was determined by employing a UV–vis spectrophotometer. Two colors, including methylene blue (MB) and erythro-sine (ET), were used for testing the $\text{Co}_3\text{O}_4/\text{CeO}_2$ nanocomposite photocatalyst activity.

Result and discussion

One of the tools for the crystallographic recognition of synthetic bulk, nano, and a thin film is XRD (Sharma et al. 2012). Figure 2 presented the XRD pattern of the $\text{Co}_3\text{O}_4/\text{CeO}_2$ nanocomposites prepared with trimesic acid as stabilizer after calcination at 700 °C for 4 h. Its appearance verifies the presence of both cubic phases of CeO_2 (JCPDS No. 34-0394, space group: Fm-3m) and Co_3O_4 (JCPDS No. 43-1003, space group: Fd3m). Also, there are no impurities detected in the pattern. Crystalline sizes are computed from Scherrer equation, $D_c = K\lambda/\beta\cos\theta$, where β is the width of the observed diffraction peak at its half maximum intensity (FWHM), K is the shape factor, which takes a value of about 0.9, and λ is the

Fig. 2 XRD pattern of $\text{Co}_3\text{O}_4/\text{CeO}_2$ nanocomposite after calcination at 700 °C for 4 h

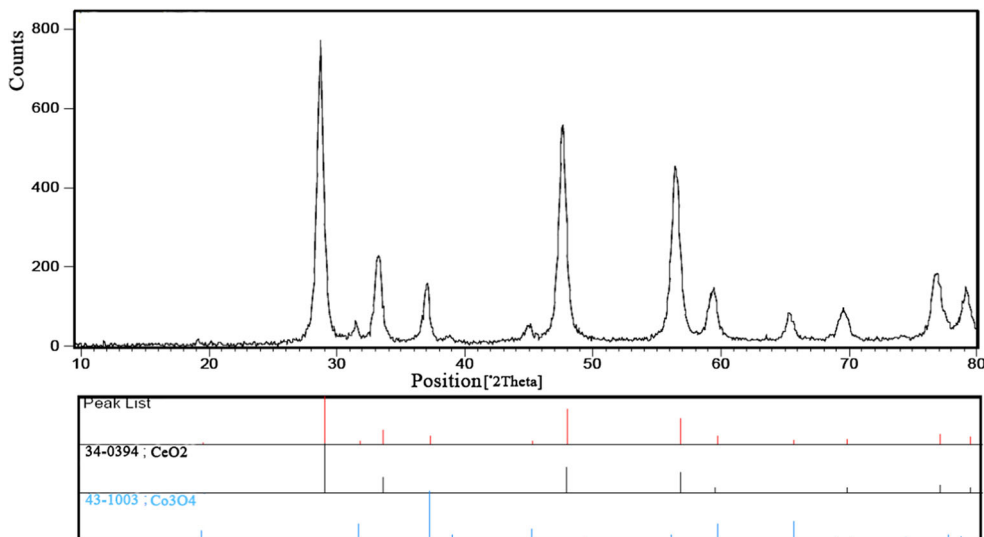
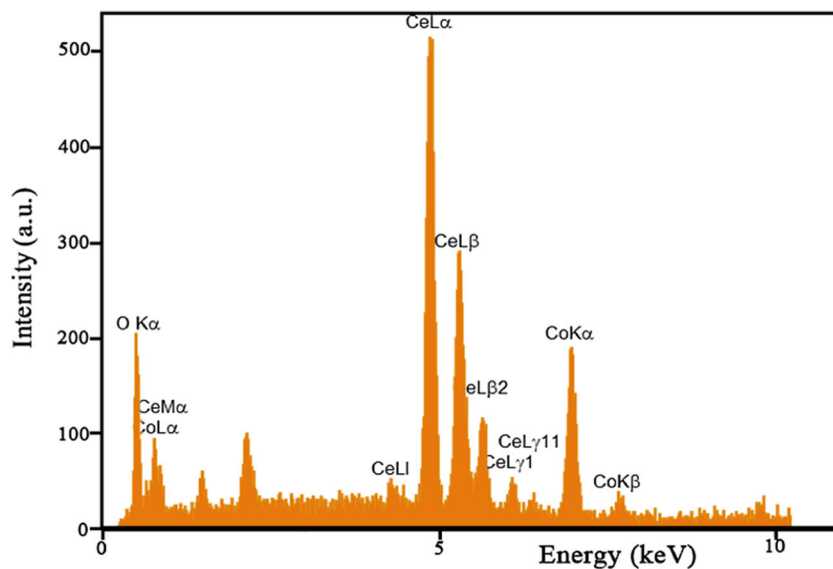


Fig. 3 EDS spectra of $\text{Co}_3\text{O}_4/\text{CeO}_2$ nanocomposite



X-ray wavelength ($\text{CuK}\alpha$ radiation, equals to 0.154 nm) (Sharma et al. 2012); the average crystalline sizes gained were about 20 nm for the $\text{Co}_3\text{O}_4/\text{CeO}_2$ nanocomposites.

For complete assurance, EDS analysis was used to corroborate the attendance of the desired elements in the resulting nanocomposites. The result, as shown in Fig. 3,

confirms the presence of cobalt, cerium, and oxygen elements. Subsequently, the EDS mapping analysis was operated to illustrate how the elements are located throughout the nanocomposites. As shown in Fig. 4, the elements of cobalt, cerium, and oxygen were distributed uniformly. Also, considering the distribution of the nanoparticles side

Fig. 4 Mapping analysis of $\text{Co}_3\text{O}_4/\text{CeO}_2$ nanocomposite

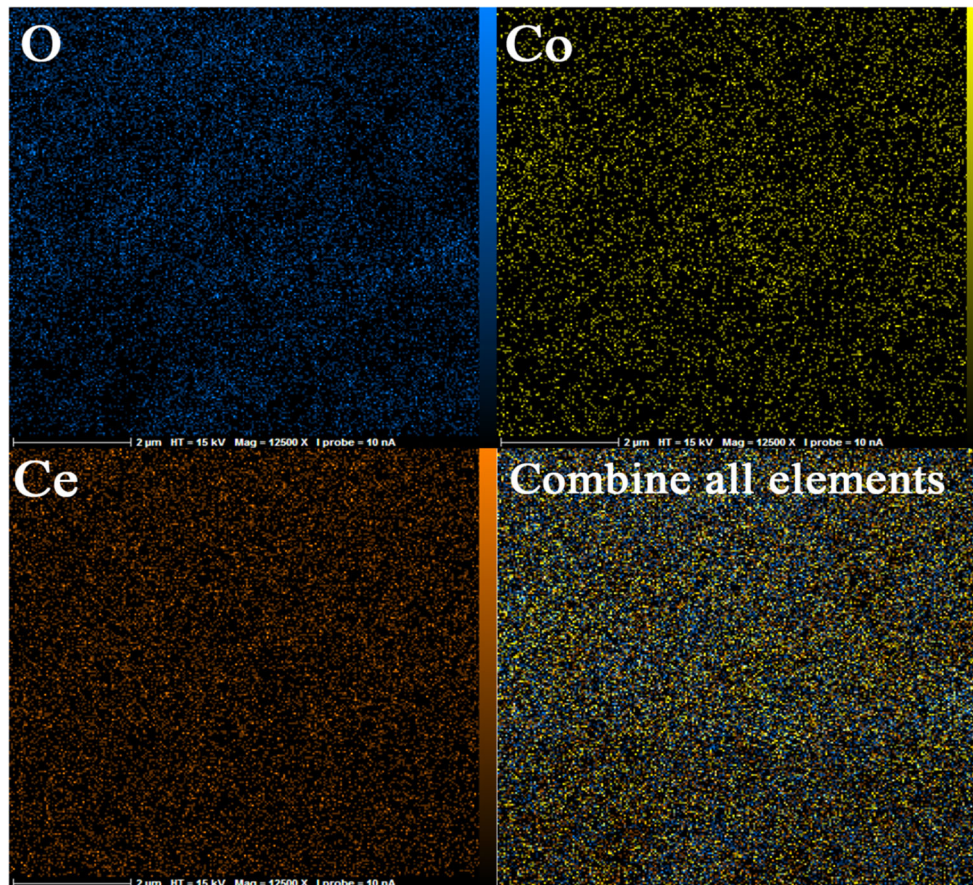


Fig. 5 FT-IR spectra of $\text{Co}_3\text{O}_4/\text{CeO}_2$ nanocomposite after calcination at $700\text{ }^\circ\text{C}$ for 4 h

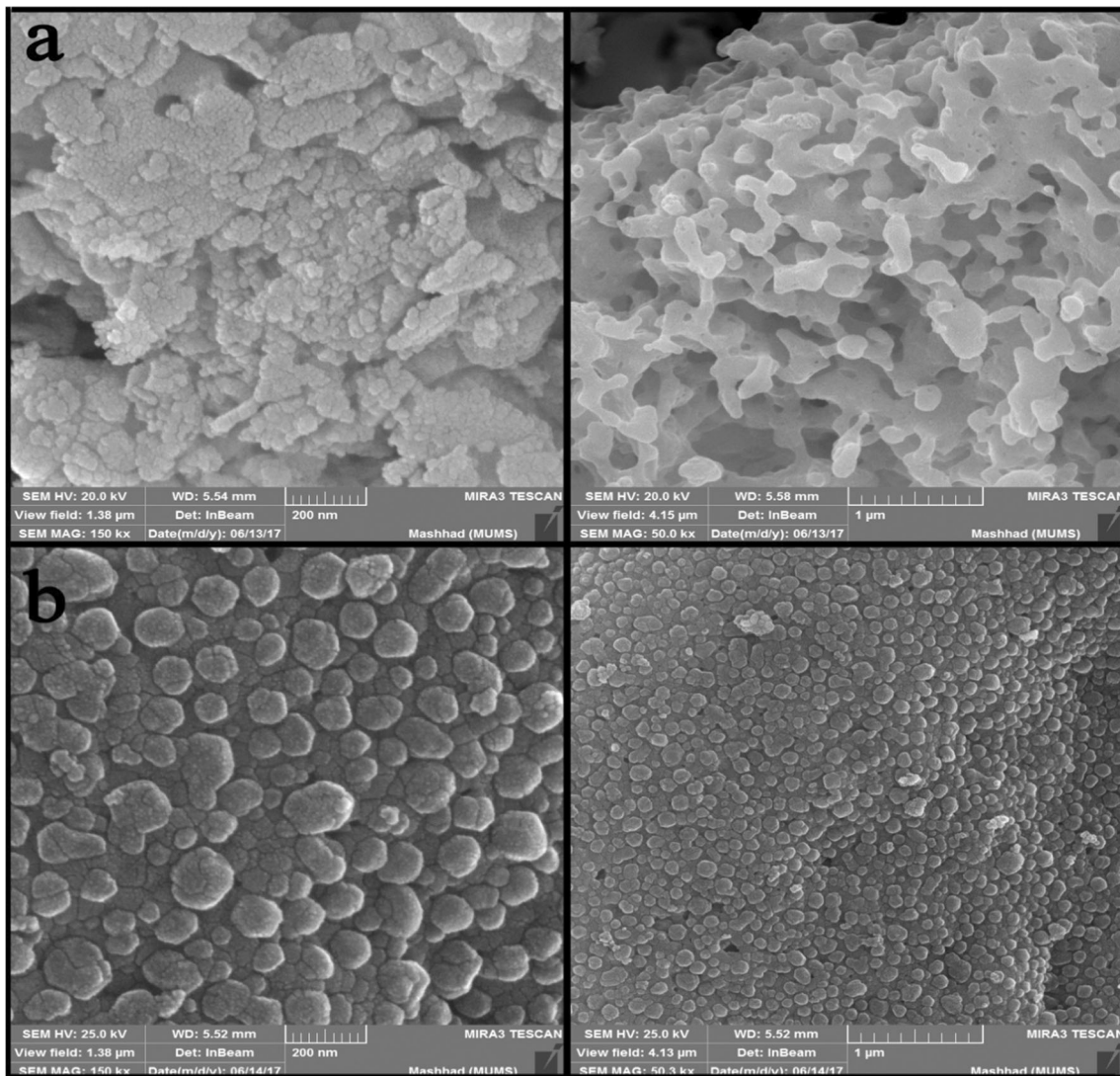
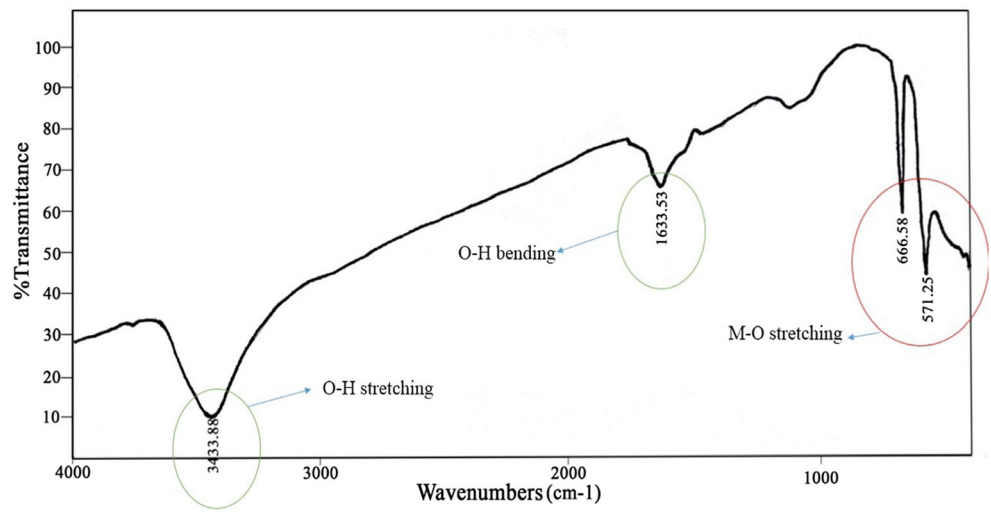


Fig. 6 SEM images of $\text{Co}_3\text{O}_4/\text{CeO}_2$ nanocomposite: (a) citric and (b) maleic acids

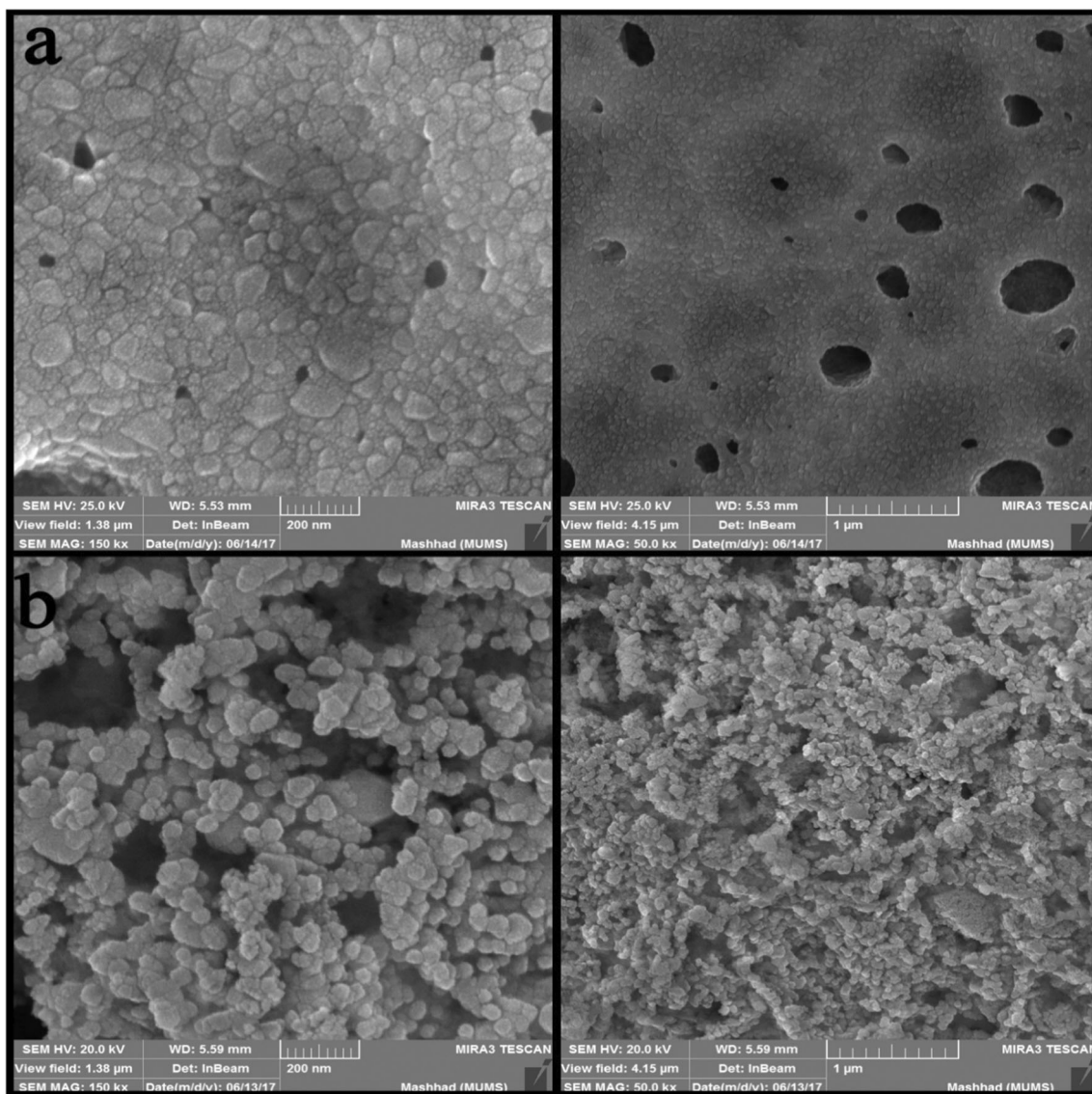
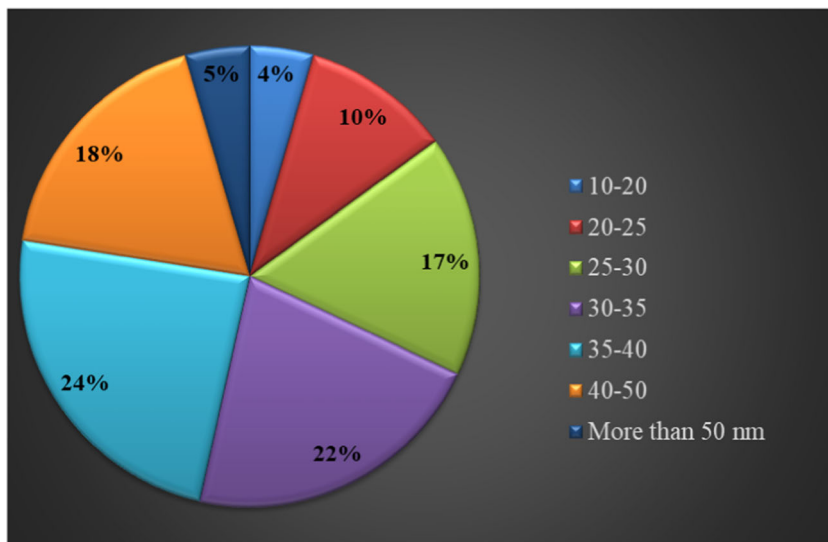


Fig. 7 SEM images of $\text{Co}_3\text{O}_4/\text{CeO}_2$ nanocomposite: (a) succinic and (b) trimesic

Fig. 8 Particle size distribution plot when trimesic is used as a stabilizer



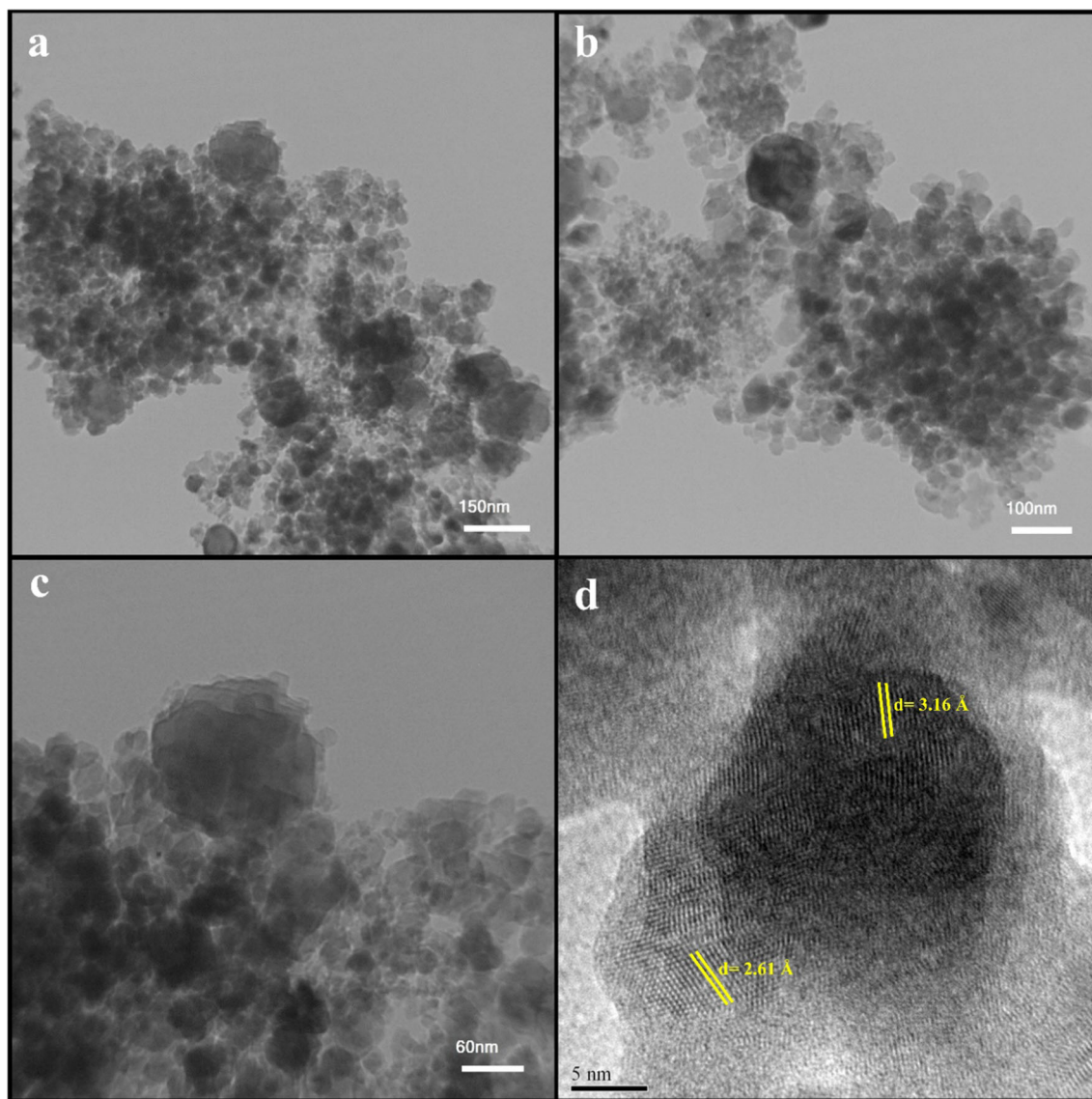


Fig. 9 (a)–(c) TEM images in different magnification and (d) HRTEM of $\text{Co}_3\text{O}_4/\text{CeO}_2$ nanocomposite that used trimesic acid as stabilizer

by side can help in interpreting the photocatalytic properties of this nanocomposite.

The FT-IR spectrum of the as-synthesized $\text{Co}_3\text{O}_4/\text{CeO}_2$ nanocomposites is illustrated in Fig. 5. The absorption peaks at 3433 and 1633 cm^{-1} related to the stretching and bending vibrational absorptions of O-H (Gharahshiran et al. 2020). The peaks at 574 and 664 cm^{-1} corresponded to the stretching vibration of $\text{Co}^{2+}\text{-O}$ and $\text{Co}^{3+}\text{-O}$, respectively (Hassanpour et al. 2017a; Salavati-Niasari et al. 2009), and a short peak around 410 cm^{-1} attributed to Ce-O (Panahi-Kalamuei et al. 2015; Ho et al. 2020).

For observation of the morphology, dispersed and agglomerated, and surface functionalization of materials in nanoscale, SEM images are suitable (Drouin et al. 2006). For studying the effects of carboxylic acid on the morphology of the synthesized nanocomposites, four carboxylic acids as

stabilizers were used. Figure 6 illustrated the SEM images of $\text{Co}_3\text{O}_4/\text{CeO}_2$ nanocomposites that used (a) citric and (b) maleic acids as stabilizers. As can be seen, when citric and maleic are used, the nanoparticles because of their high activity showed agglomeration after calcination, but the maleic one is more uniform than when citric acid was used. The SEM images obtained from samples that used succinic and trimesic are illustrated in Fig. 7. When succinic acid was used (Fig. 7a), agglomeration occurred and the formed nanoparticles stick together. The composites synthesized with trimesic acid show mono-dispersed and spherical shape (Fig. 7b). Study of the distribution of particle size for nanocomposites synthesized with trimesic acid as the stabilizer is shown in Fig. 8. The highest percentage is related to particles with 30 to 40 nm in size. Also, the average size of the nanoparticles was about 35 nm. TEM images of an optimum sample that used trimesic as

the stabilizer were taken to qualify the exact morphology and particle size of the synthesized nanocomposites. As shown in Fig. 9a–c, it is obvious that the morphology of the product is a particle. The average particle size of the TEM image is calculated at 30 nm. A high-resolution TEM image of the $\text{Co}_3\text{O}_4/\text{CeO}_2$ nanocomposites is exhibited in Fig. 9d. The crystalline planes were recognized by the parallel lines indicating the high degree of crystallinity of the nanocomposites. The lattice fringes are clearly shown with spacing fringes of 2.61 and 3.16 Å, which matched well with the crystal planes (311) and (111) of Co_3O_4 and cubic CeO_2 crystals, respectively.

One of the properties of nanomaterials that can be valuable in the study of photocatalytic virtues is its magnetic property (Wu et al. 2016), which is understood by VSM analysis. The magnetization evaluations as a function of the magnetic field are studied at 300 K and shown in Fig. 10. As is clear from the plot, $\text{Co}_3\text{O}_4/\text{CeO}_2$ nanocomposites have superparamagnetic properties. According to the graph obtained from the VMS analysis, nanocomposites have a saturation magnetization of 0.45 emu/g and a coercivity very close to zero. The lack of hysteresis loops has substantially confirmed the small size of the synthesized particles. The magnetic properties of nanocomposites for the recovery of nanoparticles from the photocatalyst test environment at the end of the work are of great interest.

The BET method is a standard tool to measure the surface area and pore volume of as-prepared samples from nitrogen adsorption isotherms measured at 77 K. Figure 11a and b shows the adsorption/desorption isotherms and BJH plots of $\text{Co}_3\text{O}_4/\text{CeO}_2$ nanocomposites, respectively. As is clear from the figure, the type III isotherm with a type H3 hysteresis loop for the nanocomposites was obtained from the BET method. Due to the type of isotherm and the hysteresis loop, funnel-

shaped cavities for these nanocomposites are probable (Ghiyasiyan-Arani and Salavati-Niasari 2018; Leofanti et al. 1998; Mobini et al. 2018). The specific surface areas, total pore volumes, and mean pore diameters obtained from the BET were $26.818 \text{ (m}^2 \text{ g}^{-1}\text{)}$, $0.1939 \text{ (cm}^3 \text{ g}^{-1}\text{)}$, and 28.927 (nm) , respectively. The data obtained from the BET analysis confirm that the increase in the percentage of decolorization after the photocatalytic process is not due to the physical absorption of the dye onto the nanoparticles.

Diffuse reflectance spectra (DRS) of $\text{Co}_3\text{O}_4/\text{CeO}_2$ nanocomposites in Fig. 12 show the optical absorption capability in the region from 200 to 800 nm. The optical energy bandgap of the nanocomposites was defined using the following relation (Hassanpour et al. 2017c):

$$(\alpha h\nu) = C(h\nu - E_g)^{1/2} \quad (1)$$

For CeO_2 , the bandgap on 2.72 (Fiorenza et al. 2018), 3.57 (Maensiri et al. 2007), and 3.35 eV (Sangsefidi and Salavati-Niasari 2017) and for Co_3O_4 1.53 and 2.02 eV (Salavati-Niasari and Khansari 2014) and 2 and 3.2 eV (Soofivand and Salavati-Niasari 2015) are reported in the literature. For this nanocomposite, two band gaps estimated for Co_3O_4 were 2.9 and 3.5 eV and the bandgap estimated for CeO_2 was 3.9 eV. The calculated band gap reveals that prepared nanocomposites can be used as a good catalyst in the photocatalytic process. To investigate the photocatalytic activity of synthesized nanocomposites, the decolorization of MB and ET in aqueous solution under UV irradiation was done. The absorption of samples is studied in the maximum wavelength obtained by the UV–vis of prepared colors, which is shown in Fig.

Fig. 10 Room temperature hysteresis loop of $\text{Co}_3\text{O}_4/\text{CeO}_2$ nanocomposite

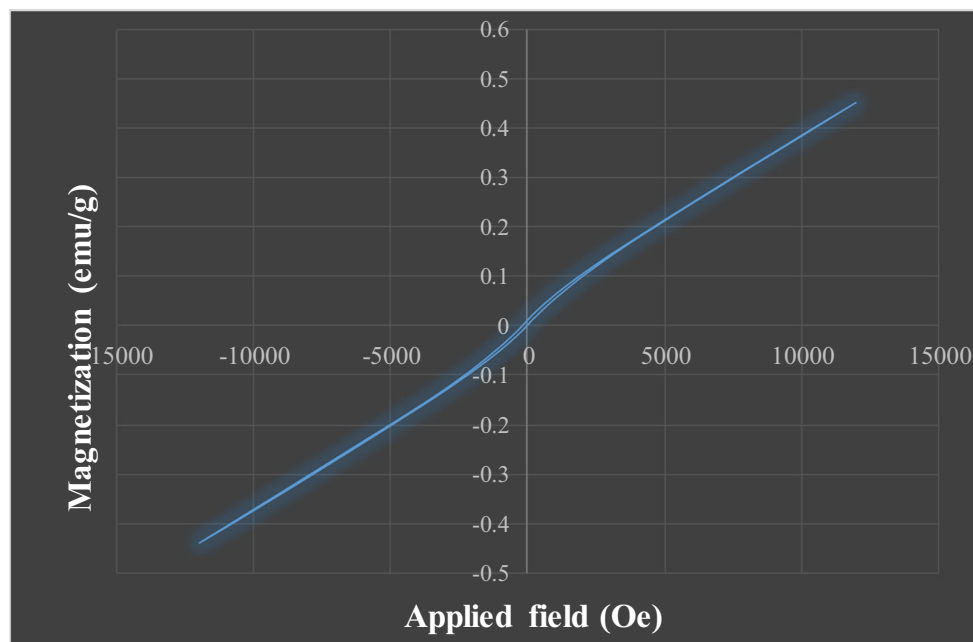
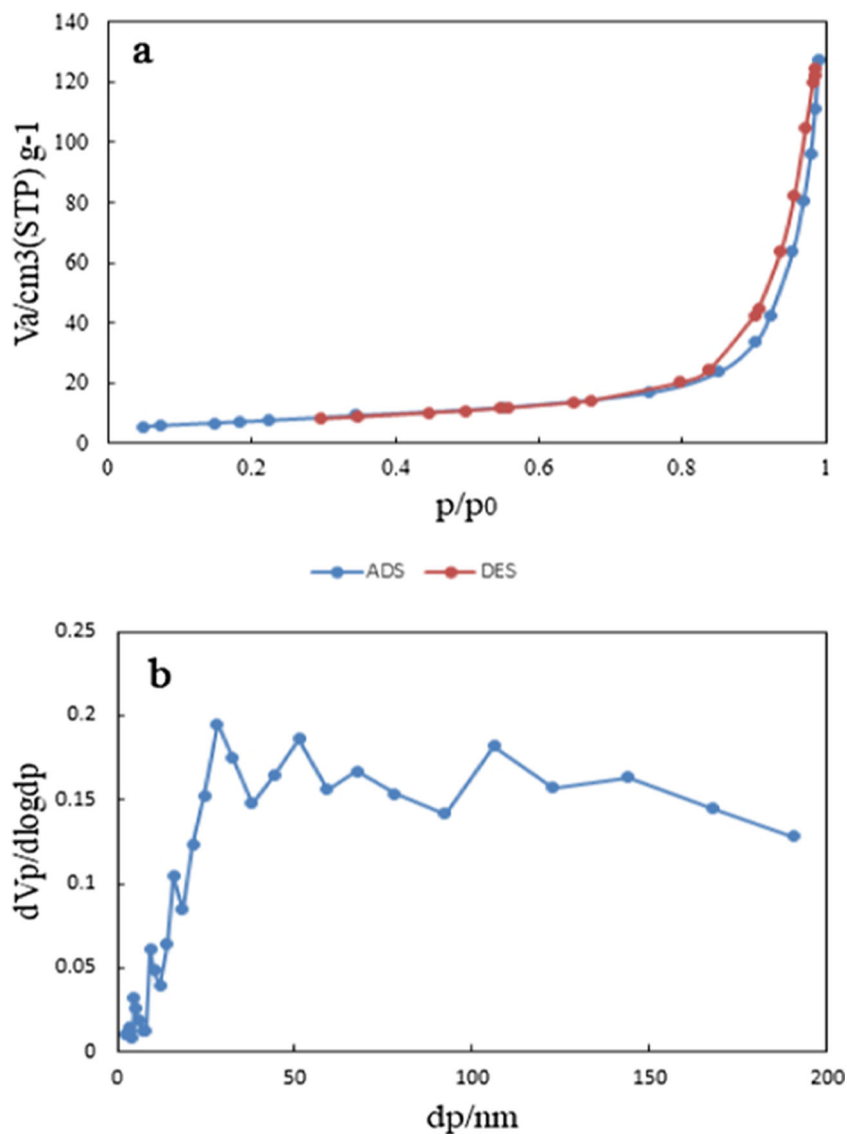


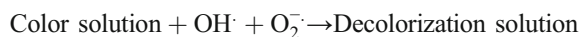
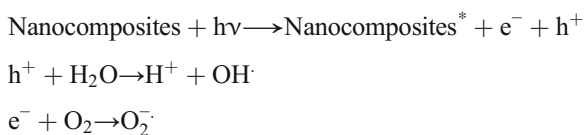
Fig. 11 (a) N₂ adsorption/desorption isotherms and (b) BJH pore size distributions of Co₃O₄/CeO₂ nanocomposite



13. Obtained lambda max for MB and ET was 620 and 484 nm, respectively. Figure 14 reveals that the prepared nanocomposites catalyze processes effectively. When pollutants are exposed to prepared Co₃O₄/CeO₂ nanocomposites and UV light, decreasing of pollutant concentration begins. The photocatalytic efficiency is calculated by the following equation (Moshtaghi et al. 2016):

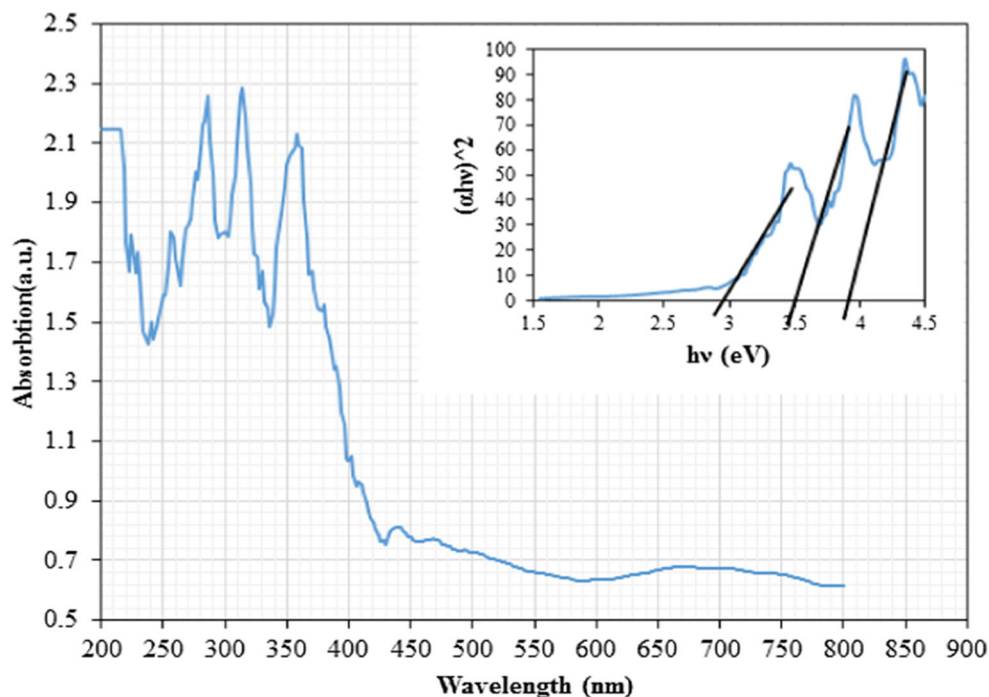
$$\text{Decolorization (\%)} = (C_0 - C_t / C_0) \times 100(2)$$

Where C₀ (mg L⁻¹) is the initial concentration of colors in solution and C_t (mg L⁻¹) is the concentration of colors at any irradiation time (min). The probable mechanism for the photocatalyst test in a water solution is as follows:



Electron-cavity pairs (e⁻ and h⁺) are formed after colliding light to nanocomposites, and the size of nanocomposite bandgap has a direct influence on its recombination rate; whenever the recombination rate is higher, there will be a possibility of increased photocatalytic activity (Wang et al. 2007; Wang et al. 2005). When each of these metal oxides is used alone, due to their bandgap, the rate of formation and recombination of the electron cavity has a specific duration. However, when two metal oxides come together after the electron cavity formation, the time of recombination alters. The reason for this change is the migration of electrons from the metal oxide conduction band with the lower bandgap to the metal oxide conduction band with higher band gap; therefore, the recombination time increases. As mentioned previously, the rate of decolorization increases with the increased recombination time and increased production of free radicals

Fig. 12 Diffuse reflectance spectra (DRS) of $\text{Co}_3\text{O}_4/\text{CeO}_2$ nanocomposite



in the aquatic environment (Magdalane et al. 2017; Sohrabnezhad and Rajabi 2018). The photocatalytic activity was measured in neutral pH, acidic, alkaline, with and without UV irradiation for a period of 120 min. When there is no irradiation, decolorization is very low for both neutral acidic and alkaline solutions. The low percentage of decolorization indicates color absorption on the surface of the catalyst. In neutral pH, percentages of decolorization were obtained about 51 and 52% decolorization for MB and ET, respectively. For better color interaction with the catalyst in the solution that contained MB as cationic color (Fil et al. 2012), ammonia was used to adjust its pH to 8, and the decolorization achieved was 85%; on the other hand, for ET as anionic color (Rithidej and Phaechamud 2003), nitric acid was used to adjust pH to 6, and the result was 90% decolorization for it. There is a raise in the

percentage of decolorization of dye after adding an acidic or alkaline agent to the media; when a cationic color that has a positive charge on its surface is used, it causes a negative charge on the surface of the catalyst, leading to better contact of color and catalyst, continuously increasing the decolorization percentage. On the basis of this, for anionic color, the process exactly reverses (Shojaei et al. 2013). To compare the results of the photocatalytic test performed, a report of the photocatalytic test results for CeO_2 and Co_3O_4 separately is provided. In literature, photocatalytic test results for CeO_2 against color solutions containing acridine orange showed about 45% (Khan et al. 2013), amido black about 45% (Khan et al. 2011), and trypan blue about 90% (Ravishankar et al. 2015). Also, for Co_3O_4 color removal in an aqueous solution containing rhodamine B about 70% (Huang et al. 2018), methyl orange about 60% (Chen et al. 2009), and methylene blue about 80% (Warang et al. 2013) have been reported.

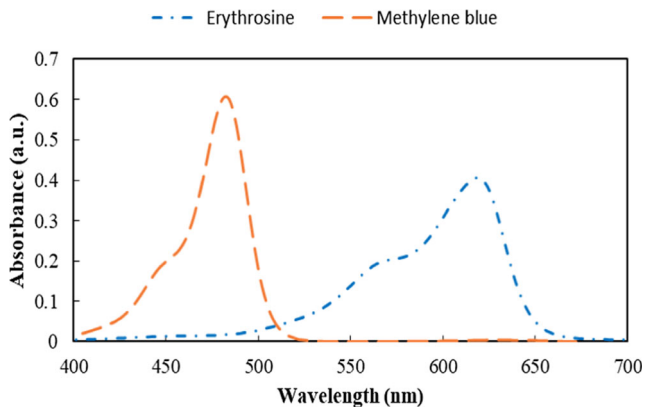
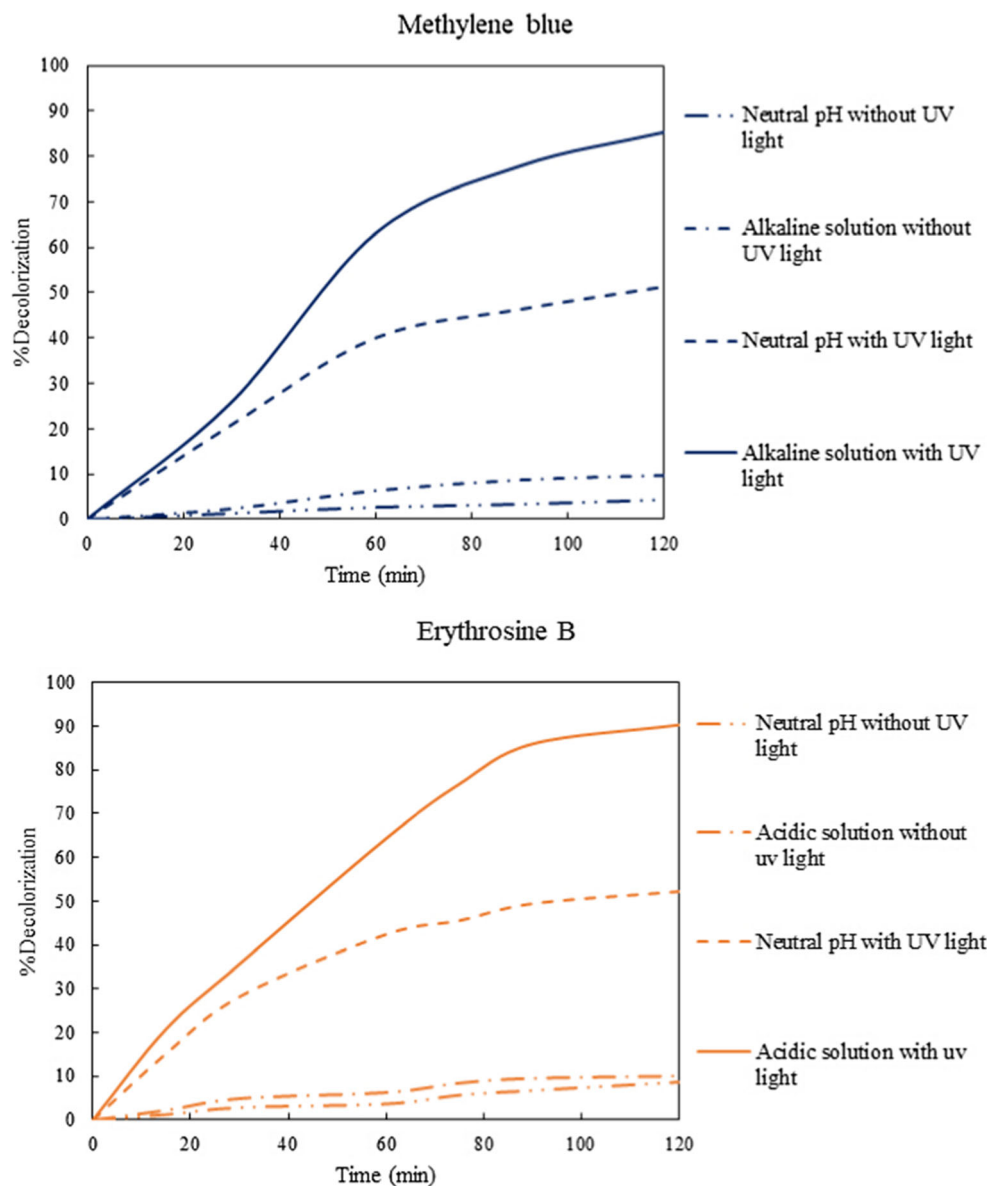


Fig. 13 UV-Vis analysis of as-prepared colors for photocatalyst test: (a) MB and (b) ET

For both dyes at optimal pH conditions and at 90 min, three different amounts of $\text{Co}_3\text{O}_4/\text{CeO}_2$ nanocomposites were used for photocatalyst testing. As shown in Fig. 15a and b, in the first step, a significant increase is observed with increasing catalyst content in the medium. But as the process progressed, the gradient of the decolorization increase was mild, with a slight difference in the decolorization rate. This indicates that the catalyst content in each photocatalyst test has an optimum value that must be considered to increase the efficiency of the photocatalyst process (Nam et al. 2002).

To examine the effect of dye concentration on the photocatalyst activity of $\text{Co}_3\text{O}_4/\text{CeO}_2$ nanocomposites, the

Fig. 14 Photocatalytic activity of $\text{Co}_3\text{O}_4/\text{CeO}_2$ nanocomposites on decolorization of methylene blue (MB) and erythrosine (ET)



test was performed at four different concentrations under optimum pH conditions and at 90 min, as illustrated in Fig. 15c and d. As the concentration of the dye used increases, the decolorization by the nanocomposite decreases. What is likely due to this event is that the decrease in light penetration with increasing color concentration causes less light to reach the catalyst to perform the photocatalytic process, thus reducing the amount of photocatalytic activity and decolorization (Kiriakidou et al. 1999).

In addition to the nanocomposite decolorization rate, other points to be noted for their photocatalytic properties are their stability and ability for repeating similar processes. To investigate the stability and repeatability of the photocatalytic activity of $\text{Co}_3\text{O}_4/\text{CeO}_2$ nanocomposites, the photocatalytic process for both dyes was optimized in four cycles under optimum pH conditions. After each step of the photocatalyst test,

the nanoparticles were recycled and used for the next cycle. As shown in Fig. 16, the nanocomposites had proper stability and repeatability over four consecutive cycles, but the changes observed in the fourth cycle were not significant compared with the first cycle.

Conclusion

As a result, $\text{Co}_3\text{O}_4/\text{CeO}_2$ nanocomposites were synthesized via a simple modified Pechini method. For the synthesis, four carboxylic acids were used, and their effects on the morphology of nanocomposites were investigated. The identification analyses were done and confirmed the purity of the synthesized nanocomposites. The sample that used trimesic acid as a stabilizer was selected as the optimal sample because of its uniform shape and

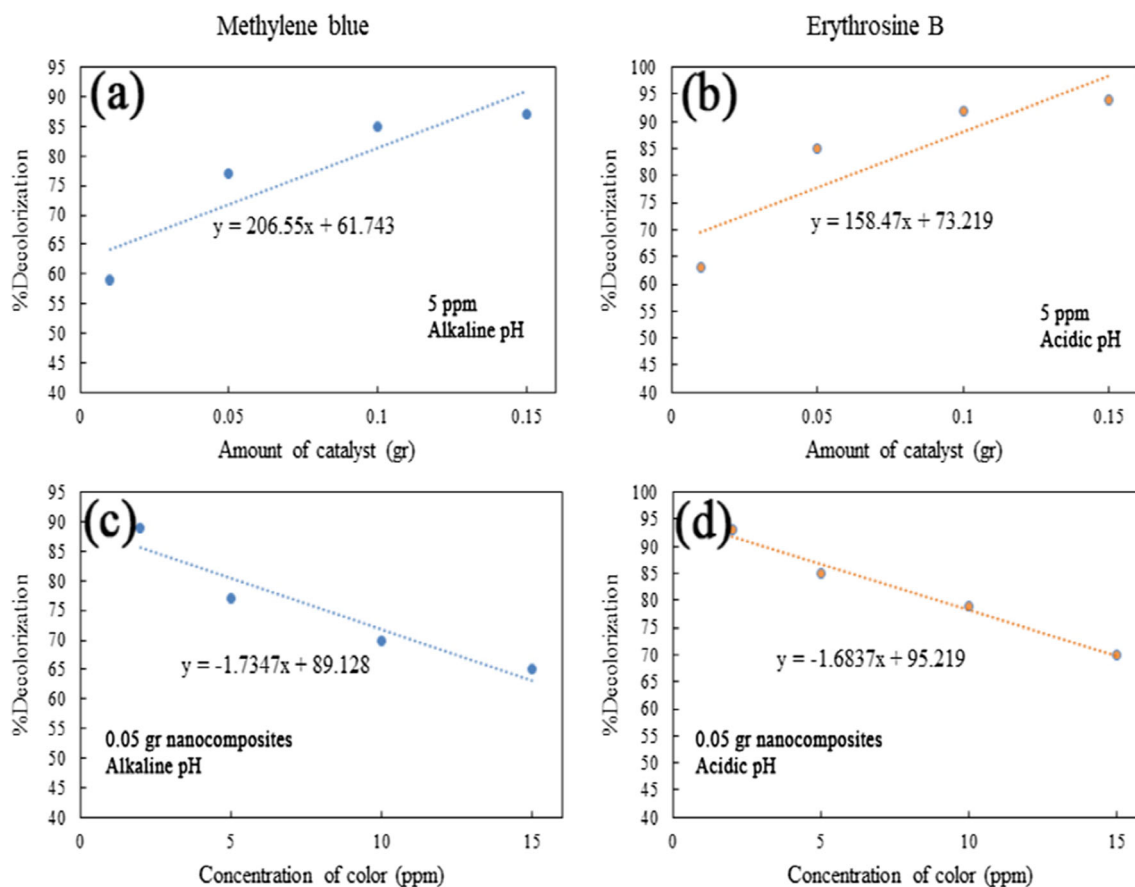
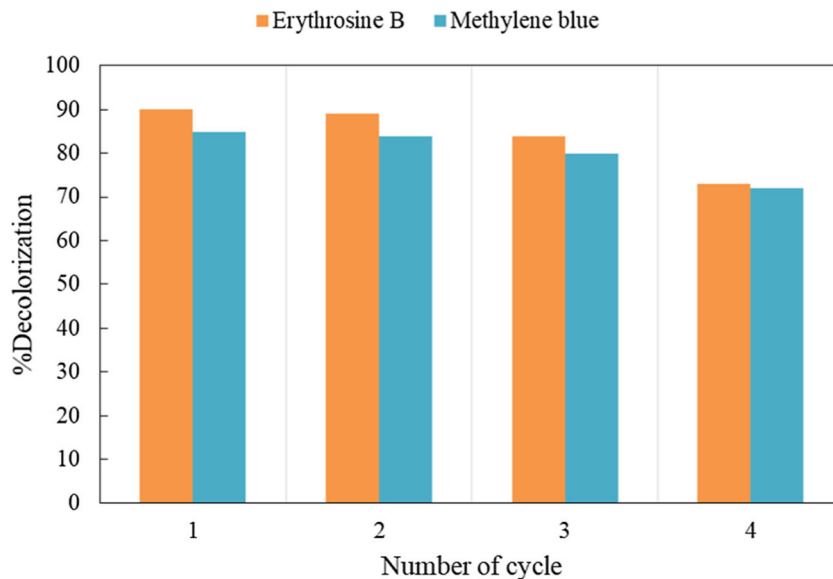


Fig. 15 The effect of amount of nanocomposites (a, b) and dye concentration (c, d) on the decolorization

small size. The selected sample was used as a photocatalyst against two aqueous solutions containing organic colors as a pollutant. The photocatalyst process was done in neutral and non-neutral media. The nanocomposite showed better performance in non-neutral media because of better interactions with

the dye. Different amounts of catalyst and different concentrations of the dye, as well as the repeatability and stability of the nanocomposite during the photocatalytic process, were investigated. Due to the photocatalyst results obtained, $\text{Co}_3\text{O}_4/\text{CeO}_2$ nanocomposite can be known as a suitable photocatalyst.

Fig. 16 The photocatalytic stability of $\text{Co}_3\text{O}_4/\text{CeO}_2$ nanocomposites in recycling reactions under the same condition



Acknowledgment The authors are grateful to the council of Iran National Science Foundation (INSF) (97017837) and the University of Kashan for supporting this work by Grant No. (159271/11).

References

- Alem S, Latifi R, Angizi S, Mohamadbeigi N, Rajabi M, Ghasali E, Orooji Y (2020) Development of metal matrix composites and nanocomposites via double-pressing double-sintering (DPDS) method. *Mater Today Commun* 25:101245
- Arefi-Oskoui S, Khataee A, Safarpour M, Orooji Y, Vatanpour V (2019) A review on the applications of ultrasonic technology in membrane bioreactors. *Ultrason Sonochem* 58:104633
- Belver C, Bedia J, Gómez-Avilés A, Peñas-Garzón M, Rodriguez JJ (2019) Semiconductor photocatalysis for water purification. *Nanoscale materials in water purification*. Elsevier, Amsterdam, pp 581–651
- Boruah PK, Borthakur P, Das MR (2019) Magnetic metal/metal oxide nanoparticles and nanocomposite materials for water purification. *Nanoscale materials in water purification*. Elsevier, Amsterdam, pp 473–503
- Chen Y, Hu L, Wang M, Min Y, Zhang Y (2009) Self-assembled Co_3O_4 porous nanostructures and their photocatalytic activity. *Colloids Surf A Physicochem Eng Asp* 336:64–68
- Dong Y, He K, Yin L, Zhang A (2007) A facile route to controlled synthesis of Co_3O_4 nanoparticles and their environmental catalytic properties. *Nanotechnology* 18:435602
- Drouin D, Pauc N, Phillips M, Poissant P, Delamplé V, Souifi A, Aimez V, Beauvais J (2006): SEM characterization of nanodevices and nanomaterials, nanoscience and nanotechnology, 2006. ICONN'06. International Conference on. IEEE
- Fernández JG, Almeida CA, Fernández-Baldo MA, Felici E, Raba J, Sanz MI (2016) Development of nitrocellulose membrane filters impregnated with different biosynthesized silver nanoparticles applied to water purification. *Talanta* 146:237–243
- Fil BA, Ozmetin C, Korkmaz M (2012) Cationic dye (methylene blue) removal from aqueous solution by montmorillonite. *Bull Kor Chem Soc* 33:3184–3190
- Fiorenza R, Bellardita M, Barakat T, Scire S, Palmisano L (2018) Visible light photocatalytic activity of macro-mesoporous $\text{TiO}_2\text{-CeO}_2$ inverse opals. *J Photochem Photobiol A Chem* 352:25–34
- Fu X, Wang C, Yu H, Wang Y, Wang T (2007) Fast humidity sensors based on CeO_2 nanowires. *Nanotechnology* 18:145503
- Fuku X, Matinise N, Masikini M, Kasinathan K, Maaza M (2018) An electrochemically active green synthesized polycrystalline NiO/MgO catalyst: use in photo-catalytic applications. *Mater Res Bull* 97:457–465
- Gharahshiran VS, Taherian Z, Khataee A, Meshkani F, Orooji Y (2020) Samarium-impregnated nickel catalysts over SBA-15 in steam reforming of CH_4 process. *J Ind Eng Chem* 86:73–80
- Ghasali E, Orooji Y, Alizadeh M, Ebadzadeh T (2020): Chromium carbide, carbon nano tubes and carbon fibers reinforced magnesium matrix hybrid composites prepared by spark plasma sintering. *Materials Science and Engineering: A*, 139662
- Ghasemi M, Khataee A, Gholami P, Soltani RDC, Hassani A, Orooji Y (2020) In-situ electro-generation and activation of hydrogen peroxide using a CuFeNLDH-CNTs modified graphite cathode for degradation of cefazolin. *J Environ Manag* 267:110629
- Ghiyasiyan-Arani M, Salavati-Niasari M (2018) Effect of $\text{Li}_2\text{CoMn}_3\text{O}_8$ nanostructures synthesized by a combustion method on montmorillonite K10 as a potential hydrogen storage material. *J Phys Chem C* 122:16498–16509
- Guo W, Sun W, Wang Y (2015) Multilayer $\text{CuO}@ \text{NiO}$ hollow spheres: microwave-assisted metal-organic-framework derivation and highly reversible structure-matched stepwise lithium storage. *ACS Nano* 9:11462–11471
- Hassandoost R, Pouran SR, Khataee A, Orooji Y, Joo SW (2019) Hierarchically structured ternary heterojunctions based on $\text{Ce}^{3+}/\text{Ce}^{4+}$ modified Fe_3O_4 nanoparticles anchored onto graphene oxide sheets as magnetic visible-light-active photocatalysts for decontamination of oxytetracycline. *J Hazard Mater* 376:200–211
- Hassanpour M, Safardoust-Hojaghan H, Salavati-Niasari M (2017a) Degradation of methylene blue and Rhodamine B as water pollutants via green synthesized $\text{Co}_3\text{O}_4/\text{ZnO}$ nanocomposite. *J Mol Liq* 229:293–299
- Hassanpour M, Safardoust-Hojaghan H, Salavati-Niasari M (2017b) Rapid and eco-friendly synthesis of NiO/ZnO nanocomposite and its application in decolorization of dye. *J Mater Sci Mater Electron* 28:1–8
- Hassanpour M, Safardoust-Hojaghan H, Salavati-Niasari M, Yeganeh-Faal A (2017c) Nano-sized CuO/ZnO hollow spheres: synthesis, characterization and photocatalytic performance. *J Mater Sci Mater Electron* 28:1–7
- Hassanpour M, Salavati-Niasari M, Safardoust-Hojaghan H, Hamadian M (2018) CeO_2/ZnO ceramic nanocomposites, synthesized via microwave method and used for decolorization of dye. *J Nanostruct* 8:97–106
- Ho CJ, Hsieh Y-J, Rashidi S, Orooji Y, Yan W-M (2020) Thermal-hydraulic analysis for alumina/water nanofluid inside a mini-channel heat sink with latent heat cooling ceiling—an experimental study. *Int Commun Heat Mass Transfer* 112:104477
- Huang Z, Zhao Y, Xu H, Zhao J (2018) Surfactant-free synthesis, photocatalytic and electrochemical property study of Co_3O_4 nanoparticles. *Mater Res Bull* 100:83–90
- Kannan S, Sundrarajan M (2014) A green approach for the synthesis of a cerium oxide nanoparticle: characterization and antibacterial activity. *Int J Nanosci* 13:1450018
- Karimi-Maleh H, Karimi F, Malekmohammadi S, Zakariae N, Esmaeili R, Rostamnia S, Yola ML, Atar N, Movagharneshad S, Rajendran S (2020a): An amplified voltammetric sensor based on platinum nanoparticle/polyoxometalate/two-dimensional hexagonal boron nitride nanosheets composite and ionic liquid for determination of N-hydroxysuccinimide in water samples. *J Mol Liq*, 113185
- Karimi-Maleh H, Shafieizadeh M, Taher MA, Opoku F, Kiarii EM, Govender PP, Ranjbari S, Rezapour M, Orooji Y (2020b) The role of magnetite/graphene oxide nano-composite as a high-efficiency adsorbent for removal of phenazopyridine residues from water samples, an experimental/theoretical investigation. *J Mol Liq* 298:112040
- Karthik K, Dhanuskodi S, Gobinath C, Prabukumar S, Sivaramakrishnan S (2018) Multifunctional properties of microwave assisted CdO-NiO-ZnO mixed metal oxide nanocomposite: enhanced photocatalytic and antibacterial activities. *J Mater Sci Mater Electron* 29:5459–5471
- Khan ST, Malik A (2019) Engineered nanomaterials for water decontamination and purification: from lab to products. *J Hazard Mater* 363:295–308
- Khan SB, Faisal M, Rahman MM, Jamal A (2011) Exploration of CeO_2 nanoparticles as a chemi-sensor and photo-catalyst for environmental applications. *Sci Total Environ* 409:2987–2992
- Khan SB, Faisal M, Rahman MM, Akhtar K, Asiri AM, Khan A, Alamry KA (2013) Effect of particle size on the photocatalytic activity and sensing properties of CeO_2 nanoparticles. *Int J Electrochem Sci* 8:7284e97
- Kiriakidou F, Kondarides DI, Verykios XE (1999) The effect of operational parameters and TiO_2 -doping on the photocatalytic degradation of azo-dyes. *Catal Today* 54:119–130
- Kumar SG, Rao KK (2017) Comparison of modification strategies towards enhanced charge carrier separation and photocatalytic

- degradation activity of metal oxide semiconductors (TiO₂, WO₃ and ZnO). *Appl Surf Sci* 391:124–148
- Kumar Reddy D, Lee S (2012) Water pollution and treatment technologies. *J Environ Anal Toxicol* 2:e103
- Leofanti G, Padovan M, Tozzola G, Venturelli B (1998) Surface area and pore texture of catalysts. *Catal Today* 41:207–219
- Li L, Yan B (2009) CeO₂-Bi₂O₃ nanocomposite: two step synthesis, microstructure and photocatalytic activity. *J Non-Cryst Solids* 355:776–779
- Li W-Y, Xu L-N, Chen J (2005) Co₃O₄ nanomaterials in lithium-ion batteries and gas sensors. *Adv Funct Mater* 15:851–857
- Li Z, Wang H, Zhao W, Xu X, Jin Q, Qi J, Yu R, Wang D (2019) Enhanced catalytic activity of Au-CeO₂/Al₂O₃ monolith for low-temperature CO oxidation. *Catal Commun* 129:105729
- Liyanaige AD, Perera SD, Tan K, Chabal Y, Balkus KJ Jr (2014) Synthesis, characterization, and photocatalytic activity of Y-doped CeO₂ nanorods. *ACS Catal* 4:577–584
- Maensiri S, Masingboon C, Laokul P, Jareonboon W, Promarak V, Anderson PL, Seraphin S (2007) Egg white synthesis and photoluminescence of platelike clusters of CeO₂ nanoparticles. *Cryst Growth Des* 7:950–955
- Magdalanee CM, Kaviyarasu K, Vijaya JJ, Siddhardha B, Jeyaraj B, Kennedy J, Maaza M (2017) Evaluation on the heterostructured CeO₂/Y₂O₃ binary metal oxide nanocomposites for UV/Vis light induced photocatalytic degradation of rhodamine-B dye for textile engineering application. *J Alloys Compd* 727:1324–1337
- Makhlouf SA (2002) Magnetic properties of Co₃O₄ nanoparticles. *J Magn Magn Mater* 246:184–190
- Mobini S, Meshkani F, Rezaei M (2018) Supported Mn catalysts and the role of different supports in the catalytic oxidation of carbon monoxide. *Chem Eng Sci* 197:37
- Moshtaghi S, Zinatloo-Ajabshir S, Salavati-Niasari M (2016) Nanocrystalline barium stannate: facile morphology-controlled preparation, characterization and investigation of optical and photocatalytic properties. *J Mater Sci Mater Electron* 27:834–842
- Mousavi SA, Hassanpour M, Salavati-Niasari M, Safardoust-Hojaghan H, Hamadani M (2018) Dy₂O₃/CuO nanocomposites: microwave assisted synthesis and investigated photocatalytic properties. *J Mater Sci Mater Electron* 29:1238–1245
- Nam W, Kim J, Han G (2002) Photocatalytic oxidation of methyl orange in a three-phase fluidized bed reactor. *Chemosphere* 47:1019–1024
- Orooji Y, Aa A, Ghasali E, Derakhshandeh MR, Alizadeh M, Asl MS, Ebadzadeh T (2019a) Co-reinforcing of mullite-TiN-CNT composites with ZrB₂ and TiB₂ compounds. *Ceram Int* 45:20844–20854
- Orooji Y, Derakhshandeh MR, Ghasali E, Alizadeh M, Asl MS, Ebadzadeh T (2019b) Effects of ZrB₂ reinforcement on microstructure and mechanical properties of a spark plasma sintered mullite-CNT composite. *Ceram Int* 45:16015–16021
- Orooji Y, Ghasali E, Moradi M, Derakhshandeh MR, Alizadeh M, Asl MS, Ebadzadeh T (2019c) Preparation of mullite-TiB₂-CNTs hybrid composite through spark plasma sintering. *Ceram Int* 45:16288–16296
- Orooji Y, Irani-nezhad MH, Hassandoost R, Khataee A, Poursan SR, Joo SW (2020) Cerium doped magnetite nanoparticles for highly sensitive detection of metronidazole via chemiluminescence assay. *Spectrochim Acta A Mol Biomol Spectrosc* 234:118272
- Panahi-Kalamuei M, Alizadeh S, Mousavi-Kamazani M, Salavati-Niasari M (2015) Synthesis and characterization of CeO₂ nanoparticles via hydrothermal route. *J Ind Eng Chem* 21:1301–1305
- Pradeep T (2009) Noble metal nanoparticles for water purification: a critical review. *Thin Solid Films* 517:6441–6478
- Qi J, Zhao K, Li G, Gao Y, Zhao H, Yu R, Tang Z (2014) Multi-shelled CeO₂ hollow microspheres as superior photocatalysts for water oxidation. *Nanoscale* 6:4072–4077
- Qi J, Lai X, Wang J, Tang H, Ren H, Yang Y, Jin Q, Zhang L, Yu R, Ma G (2015) Multi-shelled hollow micro-/nanostructures. *Chem Soc Rev* 44:6749–6773
- Qin L, Huang D, Xu P, Zeng G, Lai C, Fu Y, Yi H, Li B, Zhang C, Cheng M (2019) In-situ deposition of gold nanoparticles onto polydopamine-decorated g-C₃N₄ for highly efficient reduction of nitroaromatics in environmental water purification. *J Colloid Interface Sci* 534:357–369
- Rad TS, Ansarian Z, Soltani RDC, Khataee A, Orooji Y, Vafaei F (2020) Sonophotocatalytic activities of FeCuMg and CrCuMg LDHs: influencing factors, antibacterial effects, and intermediate determination. *J Hazard Mater* 123062:123062
- Ravishankar TN, Ramakrishnappa T, Nagaraju G, Rajanaika H (2015) Synthesis and characterization of CeO₂ nanoparticles via solution combustion method for photocatalytic and antibacterial activity studies. *ChemistryOpen* 4:146–154
- Reddy CV, Babu B, Shim J (2018) Synthesis, optical properties and efficient photocatalytic activity of CdO/ZnO hybrid nanocomposite. *J Phys Chem Solids* 112:20–28
- Rithidej GC, Phaechamud T (2003) Effect of anionic water-soluble dyes on film coating properties of chitosan acetate. *Drug Dev Ind Pharm* 29:585–594
- Salavati-Niasari M, Khansari A (2014) Synthesis and characterization of Co₃O₄ nanoparticles by a simple method. *Comptes Rendus Chimie* 17:352–358
- Salavati-Niasari M, Khansari A, Davar F (2009) Synthesis and characterization of cobalt oxide nanoparticles by thermal treatment process. *Inorg Chim Acta* 362:4937–4942
- Sangsefidi FS, Salavati-Niasari M (2017) Thermal decomposition synthesis, characterization and electrochemical hydrogen storage characteristics of Co₃O₄-CeO₂ porous nanocomposite. *Int J Hydrog Energy* 42:20071–20081
- Santhosh C, Malathi A, Dhaneshvar E, Bhatnagar A, Grace AN, Madhavan J (2019) Iron oxide nanomaterials for water purification. *Nanoscale Materials in Water Purification*. Elsevier, Amsterdam, pp 431–446
- Sharma R, Bisen D, Shukla U, Sharma B (2012) X-ray diffraction: a powerful method of characterizing nanomaterials. *Recent Res Sci Technol* 4
- Shojaei AF, Tabari AR, Loghmani MH (2013) Normal spinel CoCr₂O₄ and CoCr₂O₄/TiO₂ nanocomposite as novel photocatalysts, for degradation of dyes. *IET Micro Nano Lett* 8:426–431
- Singh S, Barick K, Bahadur D (2013) Fe₃O₄ embedded ZnO nanocomposites for the removal of toxic metal ions, organic dyes and bacterial pathogens. *J Mater Chem A* 1:3325–3333
- Sisi AJ, Fathinia M, Khataee A, Orooji Y (2020) Systematic activation of potassium peroxydisulfate with ZIF-8 via sono-assisted catalytic process: mechanism and ecotoxicological analysis. *J Mol Liq* 308:113018
- Sohrabnezhad S, Rajabi S (2018) The influence of MCM-41 mesoporous shell in photocatalytic activity of magnetic core-shell. *J Photochem Photobiol A Chem* 350:86–93
- Soofivand F, Salavati-Niasari M (2015) Co₃O₄/graphene nanocomposite: pre-graphenization synthesis and photocatalytic investigation of various magnetic nanostructures. *RSC Adv* 5:64346–64353
- Vijayakumar S, Ponnalagi AK, Nagamuthu S, Muralidharan G (2013) Microwave assisted synthesis of Co₃O₄ nanoparticles for high-performance supercapacitors. *Electrochim Acta* 106:500–505
- Wang D (2019) A critical review of cellulose-based nanomaterials for water purification in industrial processes. *Cellulose* 26:687–701
- Wang J, Zhang Z-H, Zhang X-D, Zhang L, Wang L, Xu L, Zhang P (2005) Degradation of dyestuff wastewater using visible light in the presence of a novel nano TiO₂ catalyst doped with upconversion luminescence agent. *J Environ Sci* 17:727–730
- Wang J, Pan Z, Zhang Z, Zhang X, Jiang Y, Ma T, Wen F, Li Y, Zhang P (2007) The investigation on ultrasonic degradation of acid fuchsin

- in the presence of ordinary and nanometer rutile TiO₂ and the comparison of their photocatalytic activities. *Dyes Pigments* 74:525–530
- Wang D, Yu Y, He H, Wang J, Zhou W, Abruna HD (2015) Template-free synthesis of hollow-structured Co₃O₄ nanoparticles as high-performance anodes for lithium-ion batteries. *ACS Nano* 9:1775–1781
- Wang H, Mao D, Qi J, Zhang Q, Ma X, Song S, Gu L, Yu R, Wang D (2019) Hollow multishelled structure of heterogeneous Co₃O₄-CeO_{2-x} nanocomposite for CO catalytic oxidation. *Adv Funct Mater* 29:1806588
- Warang T, Patel N, Fernandes R, Bazzanella N, Miotello A (2013) Co₃O₄ nanoparticles assembled coatings synthesized by different techniques for photo-degradation of methylene blue dye. *Appl Catal B Environ* 132:204–211
- Wei Y, Wang J, Yu R, Wan J, Wang D (2019) Constructing SrTiO₃-TiO₂ heterogeneous hollow multi-shelled structures for enhanced solar water splitting. *Angew Chem Int Ed* 58:1422–1426
- Wu T, Liu L, Pi M, Zhang D, Chen S (2016) Enhanced magnetic and photocatalytic properties of Bi₂Fe₄O₉ semiconductor with large exposed (001) surface. *Appl Surf Sci* 377:253–261
- Wutich A (2019) Water insecurity: An agenda for research and call to action for human biology. *Am J Hum Biol* 32:e23345
- Zhai Y, Zhang S, Pang H (2007) Preparation, characterization and photocatalytic activity of CeO₂ nanocrystalline using ammonium bicarbonate as precipitant. *Mater Lett* 61:1863–1866
- Zhang S, Gu P, Ma R, Luo C, Wen T, Zhao G, Cheng W, Wang X (2019) Recent developments in fabrication and structure regulation of visible-light-driven g-C₃N₄-based photocatalysts towards water purification: a critical review. *Catal Today* 335:65–77
- Zhao Y, Sun Q, Luo J, Chen H, Cai W, Su X (2018) Hydrothermal fabrication of TiO₂-MoO₃ nanocomposites with superior performance for water treatment. *Nano-Structures & Nano-Objects* 13: 93–99
- Zhu H, Jiang R, Fu Y, Guan Y, Yao J, Xiao L, Zeng G (2012) Effective photocatalytic decolorization of methyl orange utilizing TiO₂/ZnO/chitosan nanocomposite films under simulated solar irradiation. *Desalination* 286:41–48

Publisher's note Springer Nature remains neutral with regard to jurisdictional claims in published maps and institutional affiliations.